

Detection of spin pumping free of rectification and thermal artefacts in molecular-based ferromagnetic insulator $V[TCNE]_{x\sim 2}$

Zichen Wang¹, Seth Kurfman², Sarah Utsel¹, E. Johnston-Halperin^{2*}, Henning Sirringhaus¹

1.Optoelectronics Group, Cavendish Laboratory, University of Cambridge, JJ Thomson Avenue, Cambridge CB3 0HE, UK

2.Department of Physics, The Ohio State University, Columbus, OH, USA

* johnston-halperin.1@osu.edu

Abstract: The molecular-based ferrimagnetic insulator $V[TCNE]_{x-2}$ has gained recent interest for efficient spin-wave excitation due to its low Gilbert damping ratio $\alpha = 4 \times 10^{-5}$, and narrow ferromagnetic resonance linewidth $\Delta f_{FWHM} \sim 1 \text{ Oe}$. Here we report a clean spin pumping signal generated on $V[TCNE]_x$ /metal bilayer structures, free from spin rectification or thermal artifacts. On-chip coupling of microwave power is achieved via a coplanar waveguide to measure the in-plane angle-dependence of the inverse spin-Hall effect under ferromagnetic resonance conditions with respect to a constant external magnetic field. A signature of pure spin current from $V[TCNE]_x$ is observed in both platinum and permalloy metal layers, demonstrating the utility of $V[TCNE]_x$ for magnon spintronics studies in molecule/solid-state heterostructures.

Main Text

The study of spin dynamics in organic systems has drawn increasing scientific attention from physicists and chemists [1] not only because radiative recombination of spin-zero singlets leads to efficient light emission, but also due to the possibility of exploiting the spin degree of freedom for information processing [2–4]. Since the light-weight C, H, O based materials suppress spin-orbit coupling and hyperfine interaction, information carried by spins in these materials has a lifetime in microseconds [5,6], making it sufficient to undergo a series of logic operations without an additional need for error correction [7,8]. That said, the localization of electrons and holes in organic systems leads to a large conductivity mismatch between organic systems and their contacts within spintronic devices [9], causing difficulty in integrating organic materials within well-established, all-electrical, spin injection and detection architectures [7,8,10,11]. To overcome the challenge of conductivity mismatch, the promising technique of spin pumping has been proposed, where the injection of spin information across a heterogenous organic-metal boundary is based on the dissipation of angular momentum under ferromagnetic resonance condition rather than spin-polarized carrier transport across interfaces [12–16].

To date, insulating ferromagnetic yttrium iron garnet (YIG) has served as a benchmarking ferromagnetic insulator for spin-wave propagation [17,18], however, its pristine properties only show in highly crystalline and highly pure samples requiring a good lattice matching with the underlying substrates, which largely constrain its applicability [19]. An alternative low-loss molecule-based ferrimagnetic material vanadium tetracyanoethylene ($V[TCNE]_{x-2}$) has been considered for spin-wave studies following the first observation of ferromagnetic resonance by Liu. H et al [20,21]. Parallel studies demonstrated the unique capability of depositing $V[TCNE]_x$ thin films onto electrodes without detriment to its low-loss magnonic properties [22–25], thus highlighting the potential for facile on-chip integration of this magnetic material. However, despite these initial studies demonstrate a spin current generation at $V[TCNE]_x$ /Pt interface, significant question remains regarding the mechanisms behind the read-out processes – the possible contribution of magnetoresistance and thermal effects are not evaluated when the device is in continuous operation mode. The influence from these side-effects may become dominating for more complex device structures, under the condition that the spin signal is much weaker compared with direct spin pumping.

Here we performed an in-plane rotation analysis of V[TCNE]_x/metal bilayer device architecture with a series of metal layers with large spin Hall angles. The device is electromagnetically coupled to a coplanar waveguide on PCB sample holder which is also responsible for electrical connections. This compact arrangement enables the angular dependent measurement of the external field by rotation of the devices with the sample holder (shown in **Figure 1** (a)). Ferromagnetic resonance of V[TCNE]_x excites pure spin current at V[TCNE]_x/metal interface and was converted to voltage by the inverse spin Hall effect (ISHE) in the metal layer. In most of these previous measurements, the external magnetic field was confined to specific, orthogonal, orientations with respect to an external magnetic field to excite the resonance at maximum amplitude. Although most studies identify spin current detection through a Lorentzian line shape measured in the detected voltage as the magnetic field is varied [14,15,26–28], recent in-depth studies show that spurious signals originating from spin rectification can arise in the Lorentzian components from spin rectification effect (SRE) - a mixing signal between the high frequency microwave generated current and the magnetoresistance across the devices [29]. A full in-plane magnetic field rotation sweep, rather than measurements only along specified orthogonal axes, allows the identification of the true spin current and the spin rectification signal by analysis of their unique angular dependence features [13,30,31]. The result suggests V[TCNE]_x is able to excite pure spin current free from possible electrical and thermal artifacts on both platinum and permalloy interfaces, with a comparable injection efficiency to YIG. Our findings demonstrate the reliability of direct read-out of spin information at a V[TCNE]_x-metal interface, connecting the existing research in strong and weak coupling of V[TCNE]_x to RF fields with practical applications in spin-wave devices [32–34].

Spin pumping generates a pure spin current (i.e. spin flow in the absence of net charge flow) at the interface between ferromagnetic layer and insulating layer via ferromagnetic resonance (FMR) excited by external DC magnetic field \mathbf{H}_0 and AC microwave signal at specific frequency $\left(\frac{\omega}{\gamma}\right)^2 = (H_0 + 4\pi M_s)H_0$, where γ is the electron gyromagnetic ratio, M_s is the magnetization of V[TCNE]_x layer [35]. The magnitude of that spin current is given by

$$\mathbf{j}_s^{pump} = \frac{\hbar}{4\pi M_s} \left(g_r^{mix} \hat{\mathbf{m}} \times \frac{d\hat{\mathbf{m}}}{dt} - g_i^{mix} \frac{d\hat{\mathbf{m}}}{dt} \right) \quad (1)$$

, where $\mathbf{j}_s^{pump} = \mathbf{j}_\uparrow - \mathbf{j}_\downarrow$ is the spin current density, and $\hat{\mathbf{m}}$ is the unit vector of magnetization. The mixing conductance $g^{mix} = g_r^{mix} + i g_i^{mix}$ is a characteristic feature of the interface [36]. Meanwhile, spin rectification effects can be derived from the generalized Ohm's law

$$\mathbf{J} = \sigma \mathbf{E} - \frac{\sigma \Delta \rho_{AMR}}{M_s^2} [(\mathbf{j} \times \mathbf{m}) \times M_0 + (\mathbf{j} \cdot \mathbf{m}) M_0] + \sigma R_{HE} (\mathbf{J} \times \mathbf{H}) + \sigma R_{AHE} (\mathbf{J} \times \mathbf{M}) \quad (2)$$

, where second, third and fourth term describe the anisotropic magnetoresistance (AMR) effect, Hall effect (HE), and anomalous Hall effect (AHE), respectively [37].

With the DC magnetic field is rotated to an arbitrary angle φ , the measured voltage takes the form $V = V_{sym}L + V_{asym}D$

$$\begin{cases} V_{sym} = \sin \Phi (V_{AMR}^x \cos \varphi \cos 2\varphi - V_{AMR}^z \cos \varphi \sin 2\varphi) - V_{AHE} \cos \Phi \cos \varphi + V_{ISHE} \cos^3 \varphi \\ V_{asym} = -\cos \Phi (V_{AMR}^x \cos \varphi \cos 2\varphi - V_{AMR}^z \cos \varphi \sin 2\varphi) - V_{AHE} \sin \Phi \cos \varphi \end{cases} \quad (3)$$

, where L and D is the symmetric and asymmetric components of the complex Lorentz function $\frac{\Delta H/2}{(H-H_0)+i\Delta H/2}$ [38]. Most studies argue that the amplitude of symmetric Lorentz functions gives ISHE components only at the resonance condition, as the complex Lorentzian function gives the phase $\Phi = 90^\circ$ when $\mathbf{H} = \mathbf{H}_0$. However, this argument is valid only under the assumption that the RF signal \mathbf{h} and the change in magnetization $\Delta \mathbf{m}$ are at the same phase. However, P. Skalski et.al [29] suggests the existence of the possibility of a phase delay between voltage and current, and consequently, spin rectification effects enter the symmetric components. Therefore, an in-plane angle-dependent analysis should be conducted to separate the genuine spin pumping signal from the phase-delayed rectification signal.

The angular dependence of each component is plotted in **Figure 1** (b), the behaviour near 90 degrees shows a significant difference between spin rectification effects and ISHE - the detection of spin signal has $\cos^3 \varphi$ dependence, whereas the x, z components of magnetoresistance takes the form of $\sim \cos(\varphi)$ and $\sim \cos^2(\varphi)$, respectively. The additional $\cos \varphi$ dependence of ISHE reflecting the fact that the ISHE converts the spin current to the voltage perpendicular to the spin orientation (i.e. the direction of external B field). Therefore, a careful measurement of the signal near 90 degrees is crucial to distinguish between different components.

Figure 1 (c) shows the voltage measured across the metal layer V_{Device} , with perpendicular DC magnetic field and AC microwave field, original bilayer device with 1 μ m V[TCNE]_x and 7nm Pt layer produced a well-distinguished FMR absorption signal at 177.1mT, which is consistent with previous study. The Pt layer produced an ISHE signal at 0.6 μ V at 0 deg and 180 deg. In comparison with the work from N. Zhu et al [22], our FMR signal and detected voltage in Pt layer show less detailed features of higher Damon-Eshbach (DE) modes, but a broader Lorentzian peak with mode (1,1) and (3,1). The voltage across device in **Figure 1** (c) is well-fitted with a combination of a symmetric and an antisymmetric Lorentzian line shape. A small shift in peak center is present with the reversed B_0 field, we attribute this to the small out-of plane tilting angle of the device due to the roughness of the surface results from the thick encapsulation layer, as V[TCNE]_x is sensitive to the oxygen.

In order to exclude the spin rectification effect from the ISHE effects, an in-plane angular dependent analysis is performed, with the results shown in **Figure 2** (a). The extracted symmetric and asymmetric Lorentz component is then plot against the rotation angle in **Figure 2**(b). This is consistent with the fact that the asymmetric components showing the amplitude 1 order smaller. The symmetric component takes the flattened shape of $\cos(\varphi)^3$ near 90 degree, which is a signature of ISHE. The fitting according to Equation (3) gives the ISHE components of 0.598 μ V contrast to the magnetoresistance effect in x and z components with amplitude 1 order smaller, respectively. Therefore we prove that V[TCNE]_x is a suitable spin injection material with clean detection.

The g_{eff} indicating the spin injection efficiency could be evaluated from the broadening of the ferromagnetic absorption peak (with V[TCNE]_x layer thickness of $d = 1\mu m$ and $4\pi M_s = 100G$) as $\alpha_{eff} = \alpha_0 + \frac{g\mu_B}{4\pi M_s d} g_{eff}$, which gives $g_{eff} = 4.87 \times 10^{18} m^{-2}$ comparable to YIG.

However, the measured ISHE voltage is surprisingly low – according to Equation (1), the injected spin current pumped has the $\propto 1/M_s$ dependence on the magnetization of the ferromagnetic layer, therefore V[TCNE]_x should have an enhanced performance compared to YIG. However, we address the existence of the thick encapsulation layer between V[TCNE]_x layer and coplanar waveguide affects the electromagnetic coupling. According to the simulation, the effective Q factor reduced to 168 (contrasts to ~ 2000 in resonance in cavity with the presence of Pt conductive sheet), which explains the reduction in spin current.

Aside from the spin rectification effects, thermal effect is also widely argued to be another artifact for the observed signal. For the magnon-based insulators, the propagation and scattering of the magnons may cause non-uniform temperature distribution on the interface, and hence affect the chemical potential distribution [39,40]. We first study the excited magnon modes under different RF power supplied by the coplanar waveguide set-up (shown in **Figure 2** (c)) Damon-Eshbach modes (3,1) and (5,1) present together with the uniformly resonant (1,1) mode. With the increased RF power, both (3,1) and (5,1) modes increase in intensity relative to the (1,1) mode, resulting in a broader peak with combined (1,1) and (3,1) modes. As the peak width in FMR spectra matches the width in voltage measured across the Pt layer, we argue that both (1,1) and (3,1) contribute to the spin pumping around our measurement condition of 20dBm microwave power. The inset shows the increase in RF power gives linear increase in FMR absorption power as well as the voltage across the device around 20dBm (fluctuation below 14dBm is due to errors in fitting). This trend is also consistent with the observation from ref [20]. However, this is not sufficient to exclude the possible thermal effects, as both the spin current injection (following equation (1)) and thermal effects could result in the similar linear dependence on absorption power. In order to evaluate the thermal effect, we insert a 15nm Al₂O₃ layer between V[TCNE]_x and Pt bilayer structure by atomic layer deposition, so that the exchange coupling VTCNE and Pt layers are isolated while the temperature gradient is still able to propagate to the next layer. As shown in **Figure 2** (d), the signal is blocked after the insertion of Al₂O₃ layer. This fully excludes the possible thermal effects caused by the dominating (1,1) and (3,1) modes, however, we alert the readers that with higher microwave power or stronger electromagnetic coupling, thermal effects from higher excitation modes may still exists.

To further verify the origin of the signal, Permalloy (Py) is also tried. Py is a well-known ferromagnetic metal, however, it also exhibits a certain angle of spin Hall-angle [13]. According to the reported resonant peak of permalloy should occur at 18mT, well separated from the 128mT peak from the resonance. This enabled the Py layer to be used as detection layer when V[TCNE]_x is excited at resonance at $B_0 = 128mT$. **Figure 3** shows the angular dependency of the detected voltage across Py layer (normalized by absorption power against V[TCNE]_x/Pt device, so that the amplitude is comparable with V[TCNE]_x/Pt interface). Similar to the V[TCNE]_x/Pt structure, both (1,1) and (3,1) peaks present in FMR absorption and ISHE

signals. The amplitude of detected voltage across Py is $0.4\mu V$, slightly lower than the V[TCNE]_x/Pt devices. A well-distinguished ISHE peak is still observed with V[TCNE]_x/Py structure, despite the spin rectification shares larger of components. The absorption peak is broadening from V[TCNE]_x/Py structure providing an increased extracted effective mixed conductance $g_{eff} = 9.10 \times 10^{18} m^{-2}$. Providing spin Hall angle of $\theta_{SH}(Pt) = 0.014$ and $\theta_{SH}(Py) = 0.005$ measured in YIG, the difference in effective conductance could be explained by the difference in reflected spin current from the bottom of metal layer. This finding suggests the ISHE signal generated at multiple interfaces with similar injection efficiency $g^{\uparrow\downarrow}$ at interfaces, highlighting the future potentials of V[TCNE]_x applications in complex organic spintronics systems.

Conclusion

In this work, we have demonstrated spin generation and detection with bilayer devices that integrate magnet insulator V[TCNE]_x. We show evidence that by using V[TCNE]_x as a magnetic generator of spins, and on account of its very low conductivity, the measurement of the voltage signals within the device are free from electrical and thermal artifacts. Measurements based on an in-plane magnetic field rotation were performed to exclude the possible influence of spin rectification effects in the detection of spin currents generated within V[TCNE]_x/Pt bilayer devices. The possible thermal effect caused by spin wave generation were scrutinised through RF power sweeps and by swapping the non-magnet detection layer, to provide further confirmation of our artefact free measurements. Although the efficiency of spin pumping in this demo is not very high with the presence of the encapsulation layer, the successful generation of spin current in permalloy, and the successful suppression of the spurious artefacts shows the potential of V[TCNE]_x within devices that generate and transmit spin signals across interfaces. Our work spotlights the potency that organic systems hold in the field of spintronics, and in the race to construct building blocks for spin-based, dissipation-free, generation and transport of information.

Acknowledgements

The authors gratefully acknowledge funding from the European Research Council (ERC) through a Synergy Grant (Grant Agreement ID: 610115). Z.W. acknowledges the Trinity college in Cambridge for supporting his Ph.D. study. The authors express their great thanks to Dr Deepak Venkateshvaran for his generous sharing of his idea on this project.

References

- [1] Nature Materials 2009 8:9 **8**, 691 (2009).
- [2] S. Gorgon et al., Nature 2023 620:7974 **620**, 538 (2023).
- [3] K. V. Raman et al., Nature 2013 493:7433 **493**, 509 (2013).
- [4] S. Schott, E. R. McNellis, C. B. Nielsen, H. Y. Chen, S. Watanabe, H. Tanaka, I. McCulloch, K. Takimiya, J. Sinova, and H. Siringhaus, Nature Communications 2017 8:1 **8**, 1 (2017).
- [5] S. Schott et al., Nature Physics 2019 15:8 **15**, 814 (2019).
- [6] Z. G. Yu, Physical Review Letters **106**, 106602 (2011).
- [7] A. Hirohata, K. Yamada, Y. Nakatani, L. Prejbeanu, B. Diény, P. Pirro, and B. Hillebrands,

- Journal of Magnetism and Magnetic Materials **509**, 166711 (2020).
- [8] B. Dieny et al., (1928).
- [9] T. L. A. Tran, T. Q. Le, J. G. M. Sanderink, W. G. Van Der Wiel, and M. P. De Jong, *Advanced Functional Materials* **22**, 1180 (2012).
- [10] O. M. J. Van'T Erve, A. L. Friedman, E. Cobas, C. H. Li, A. T. Hanbicki, K. M. McCreary, J. T. Robinson, and B. T. Jonker, *Journal of Applied Physics* **113**, 17 (2013).
- [11] X. Lin, W. Yang, K. L. Wang, and W. Zhao, *Nature Electronics* 2019 2:7 **2**, 274 (2019).
- [12] K. Ando, S. Takahashi, J. Ieda, H. Kurebayashi, T. Trypiniotis, C. H. W. Barnes, S. Maekawa, and E. Saitoh, *Nature Materials* 2011 10:9 **10**, 655 (2011).
- [13] S. W. Jiang, S. Liu, P. Wang, Z. Z. Luan, X. D. Tao, H. F. Ding, and D. Wu, (2015).
- [14] M. Kimata, D. Nozaki, Y. Niimi, H. Tajima, and Y. Otani, *Physical Review B - Condensed Matter and Materials Physics* **91**, 224422 (2015).
- [15] S. J. Wang et al., *Nature Electronics* 2019 2:3 **2**, 98 (2019).
- [16] M. Groesbeck et al., *Physical Review Letters* **124**, 067702 (2020).
- [17] H. Y. Yuan, Y. Cao, A. Kamra, R. A. Duine, and P. Yan, *Physics Reports* **965**, 1 (2022).
- [18] L. J. Cornelissen, J. Liu, R. A. Duine, J. Ben Youssef, and B. J. Van Wees, *Nature Physics* **11**, 1022 (2015).
- [19] G. Schmidt, C. Hauser, P. Trempler, M. Paleschke, and E. T. Papaioannou, *Physica Status Solidi (B) Basic Research* **257**, (2020).
- [20] H. Liu et al., *Nature Materials* **17**, 308 (2018).
- [21] J. S. Bola, H. Popli, R. M. Stolley, H. Liu, H. Malissa, O. Kwon, C. Boehme, J. S. Miller, and Z. V. Vardeny, *Advanced Functional Materials* 2100687 (2021).
- [22] N. Zhu, X. Zhang, I. H. Froning, M. E. Flatté, E. Johnston-Halperin, and H. X. Tang, *Appl. Phys. Lett* **109**, 82402 (2016).
- [23] H. Yu, M. Harberts, R. Adur, Y. Lu, P. C. Hammel, E. Johnston-Halperin, and A. J. Epstein, *Applied Physics Letters* **105**, (2014).
- [24] A. H. Trout, S. W. Kurfman, Y. Shi, M. Chilcote, M. E. Flatté, E. Johnston-Halperin, and D. W. McComb, *APL Materials* **10**, 81102 (2022).
- [25] A. Franson, N. Zhu, S. Kurfman, M. Chilcote, D. R. Candido, K. S. Buchanan, M. E. Flatté, H. X. Tang, and E. Johnston-Halperin, *APL Materials* **7**, (2019).
- [26] Y. Tani, Y. Teki, and E. Shikoh, *Appl. Phys. Lett* **107**, 242406 (2015).
- [27] S. Watanabe, K. Ando, K. Kang, S. Mooser, Y. Vaynzof, H. Kurebayashi, E. Saitoh, and H. Siringhaus, *NATURE PHYSICS* | **10**, (2014).
- [28] D. Sun, K. J. Van Schooten, M. Kavand, H. Malissa, C. Zhang, M. Groesbeck, C. Boehme, and Z. V. Vardeny, *Nature Materials* 2016 15:8 **15**, 863 (2016).
- [29] P. Skalski, O. Zadorna, D. Venkateshvaran, and H. Siringhaus, *Physical Review Materials* **6**, 024601 (2022).
- [30] Y. Liu, Z. Xu, L. Liu, K. Zhang, Y. Meng, Y. Sun, P. Gao, H.-W. Zhao, Q. Niu, and J. Li, (n.d.).
- [31] Y. Wang, M. M. Decker, T. N. G. Meier, X. Chen, C. Song, T. Grünbaum, W. Zhao, J. Zhang, L. Chen, and C. H. Back, (n.d.).
- [32] S. W. Kurfman, D. R. Candido, B. Wooten, Y. Zheng, M. J. Newburger, S. Cheng, R. K. Kawakami, J. P. Heremans, M. E. Flatté, and E. Johnston-Halperin, (2023).
- [33] Q. Xu, H. Fung, H. Cheung, D. S. Cormode, T. O. Puel, H. Yusuf, M. Chilcote, M. E. Flatté,

- E. Johnston-Halperin, and G. D. Fuchs, (2022).
- [34] S. W. Kurfman et al., (2023).
- [35] H. Nakayama, K. Ando, K. Harii, T. Yoshino, R. Takahashi, Y. Kajiwara, K. Uchida, Y. Fujikawa, and E. Saitoh, PHYSICAL REVIEW B **85**, 144408 (2012).
- [36] Y. Tserkovnyak, A. Brataas, and G. E. W. Bauer, Physical Review Letters **88**, 117601 (2002).
- [37] M. Harder, Z. X. Cao, Y. S. Gui, X. L. Fan, and C. M. Hu, Physical Review B - Condensed Matter and Materials Physics **84**, 054423 (2011).
- [38] W. T. Soh, B. Peng, and C. K. Ong, Journal of Physics D: Applied Physics **47**, 285001 (2014).
- [39] T. An et al., Nature Materials **12**, (2013).
- [40] O. Wid, J. Bauer, A. Müller, O. Breitenstein, S. S. P. Parkin, and G. Schmidt, Nature Publishing Group (2016).

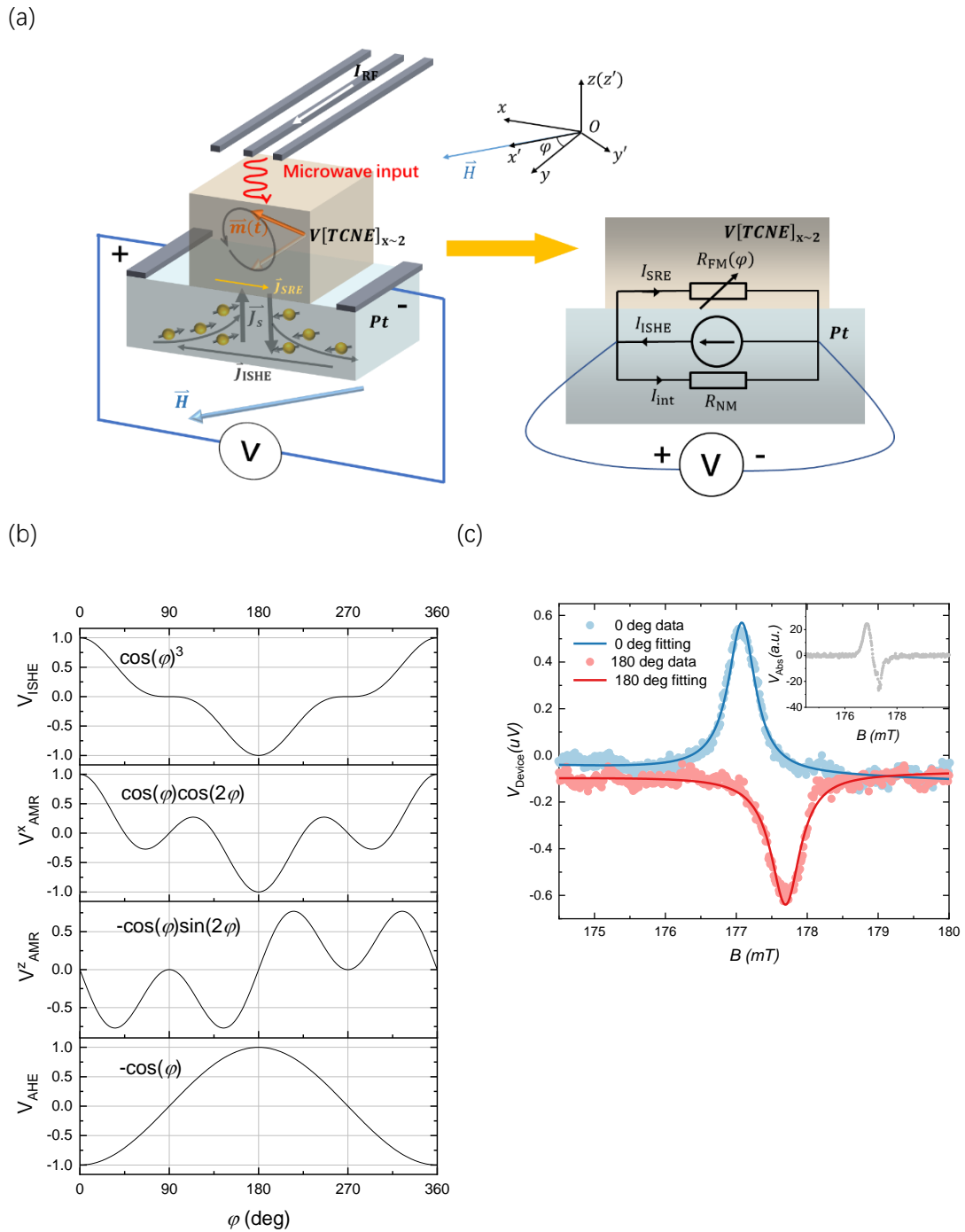


Figure 1. Measurement schematic and voltage components of the measured signal within ferromagnet-nonmagnet bilayers. (a) Experimental set-up with illustration of the spin pumping processes, (x,y,z) is the coordinate system rotating with device, (x',y',z') is the static lab coordinate system, the equivalent circuit shows the origin of spin rectification effects, (b) illustration of the shapes of angular dependence functions corresponding to difference components from voltage measured across the metal layer, (c) measured voltage across metal layer V_{device} from $V[TCNE]_x/Pt$ sample at 0 and 180 degree with Lorentzian fitting of the signal under drive from 4GHz, 20dBm RF signal, inset: absorption power from the coplanar wave guide recorded in voltage from lock-in amplifier.

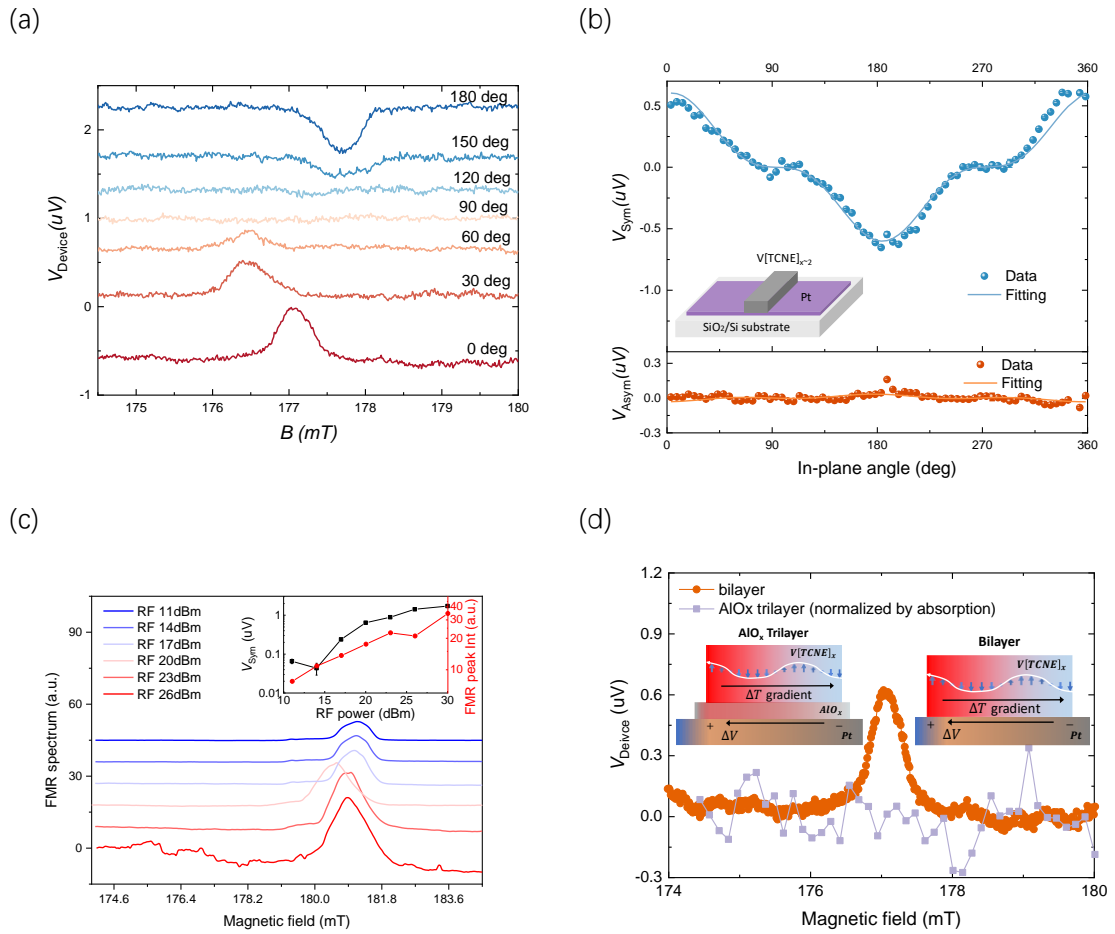


Figure 2. Angular dependence of measured voltages, and the suppression of possible artifacts within $V[TCNE]_x$ /non-magnet bilayer devices (a) voltage across metal layer V_{device} versus external B field on various in-plane rotation angles, (b) symmetric and asymmetric components of V_{device} versus in-plane rotation angle, inset: $V[TCNE]_x$ /Pt device structure (c) RF power dependence of the absorption peak and V_{device} , inset: recorded FMR peak intensity and symmetric components from V_{device} with increasing RF power, measured at 0 degree (d) V_{device} v.s. external DC B field in $V[TCNE]_x/AIO_x/Pt$ trilayer devices, inset: illustration of thermal influences on V_{device}

(a)

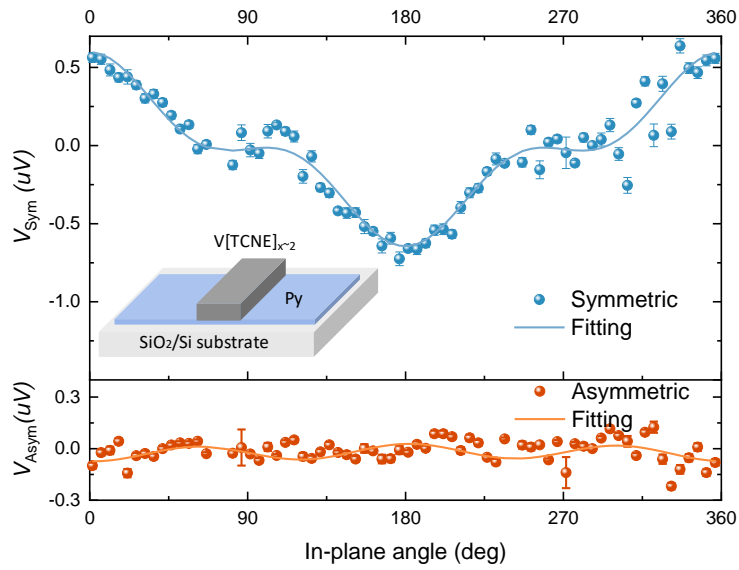


Figure 3. Additional confirmation of the suppression of spin rectification using bilayers of $V[TCNE]_x$ and the conductive magnet permalloy as a replacement for platinum. Symmetric and asymmetric components of measured voltage across the metal V_{device} v.s. in-plane rotation angle in $V[TCNE]_x/Py$ bilayer devices, with the amplitude normalized by the FMR amplitude (set FMR amplitude of $V[TCNE]_x/Pt$ in Figure 1(d) as unit 1, so that the results is comparable with Figure 2) inset: $V[TCNE]_x/Py$ bilayer device structure

Detection of spin pumping free of rectification and thermal artefacts in molecular-based ferromagnetic insulator

$V[\text{TCNE}]_{x-2}$

Supplementary Material

Zichen Wang, Seth Kurfman, Sarah Ursel, E. Johnston-Halperin, Henning Sirringhaus

Device Fabrication

The sample is fabricated on 3mm*5mm SiO₂/Si substrates. The sample is cut into dices by dice saw with the surface covered by photoresists. Then the substrate is cleaned by rinsing in Acetone, followed by sonication in Decon90, deionized water, acetone, isopropanol for 5min each. Then the surface is activated by 300W plasma ashing for 10min. The Pt film is coated by magnetron sputtering with 50W RF power in a vacuum of 3E-6 mBar. The permalloy film is coated by thermal evaporation under a vacuum of 3E-6 mBar.

<VTCNE fabrication >

Our previous ferromagnetic characterization shows that the inhomogeneous broadening of $V[\text{TCNE}]_x$ between different metal surfaces and flat SiO₂ surface is negligibly small.

Measurement set-up of the in-plane rotation

The measurements for ferromagnetic resonance (FMR) absorption and DC ISHE voltage run in parallel. The FMR measurement operates in lock-in detection scheme, enabling sensitive detection of small absorption signals - A small low frequency (19.347Hz) 0.1V AC current is applied to the electromagnet, creating an AC magnetic field in addition to the DC field. Modulated by this field, the voltage drop across the coplanar waveguide would also vary, with amplitude proportional to the derivative of the absorption curve. The voltage is amplified by a diode, then fed into a SR830 lock-in amplifier. The lock-in amplifier extracts the AC component with same frequency by multiplication of the target signal with a reference signal. The measured signal is proportional to the derivative of the FMR absorption curve. The recorded unit is in volts, however, its relationship with the power absorption is not easy to determine. In the measurement, we keep the set-up parameters unchanged, so that the is FMR amplitudes between different samples are still comparable.

The sample device is mounted to the PCB contact pad by silver conductive paste, allowing coplanar waveguide passing through in the centre.

<Coplanar waveguides>



Figure S4 Details about the sample holder design of physical layout

More details about the in-plane angle dependency of each component

Spin pumping generates pure spin current at the interface between ferromagnetic layer and insulating layer via ferromagnetic resonance (FMR) excited by external DC magnetic field \mathbf{H} and AC microwave signal \mathbf{h} . The dynamic behaviour of the magnetic moments under external fields could be modelled by the semi-classical Landau-Lifshitz-Gilbert (LLG) Equation

$$\frac{d\mathbf{M}}{dt} = -\gamma\mathbf{M} \times \mathbf{H} + \frac{\alpha}{4\pi M_s} \mathbf{M} \times \frac{d\mathbf{M}}{dt} \quad (4)$$

, where γ is electron gyromagnetic ratio and α is a material-dependent damping ratio. The first term of $-\gamma\mathbf{M} \times \mathbf{H}$ is the precession term, while the second damping term $-\frac{\alpha}{M} \mathbf{M} \times \frac{d\mathbf{M}}{dt}$ describes the relaxation of the spin, accounting for the fact that \mathbf{M} would finally aligned with \mathbf{H}_{eff} after a long period of time. By application of AC driving electromagnetic field $\mathbf{H}(\mathbf{t}) = \mathbf{H} + \mathbf{h}e^{-i\omega t}$ at specific frequency according to Kittel formula

$$\left(\frac{\omega}{\gamma}\right)^2 = (H_0 + 4\pi M_s)H_0 \quad (5)$$

\mathbf{M} will be excited in a resonant state. When $\alpha \ll 1$, the AC susceptibility of the ferromagnetic layer with various DC magnetic field \mathbf{H} is derived as $\Delta\mathbf{m} = \chi(H)\mathbf{h}$ [37]

$$\chi(H) = \frac{\frac{\Delta H}{2}}{(H - H_0) + i\frac{\Delta H}{2}} \begin{pmatrix} A_{xx} & iA_{xy} & 0 \\ -iA_{xy} & A_{yy} & 0 \\ 0 & 0 & 0 \end{pmatrix} \quad (6)$$

$$\begin{cases} A_{xy} = \frac{-4\pi M_s}{\alpha(2H_0 + 4\pi M_s)} \\ A_{xx} = -\frac{A_{xy}\gamma(H_0 + 4\pi M_s)}{\omega} \\ A_{yy} = -\frac{A_{xy}\gamma H_0}{\omega} \end{cases} \quad (7)$$

, where $\Delta\mathbf{m}$ is the variation in magnetization of the ferromagnetic layer. Then a pure spin current is generated at the interface between the ferromagnetic layer and non-magnetic layers is known as

$$\mathbf{j}_s^{pump} = \frac{\hbar}{4\pi M_s} \left(g_r^{mix} \hat{\mathbf{m}} \times \frac{d\hat{\mathbf{m}}}{dt} - g_i^{mix} \frac{d\hat{\mathbf{m}}}{dt} \right) \quad (8)$$

, where $\mathbf{j}_s^{pump} = \mathbf{j}_\uparrow - \mathbf{j}_\downarrow$ is the spin current density, and $\hat{\mathbf{m}}$ is the unit vector of magnetization.

In our bilayer device layout, the first $\hat{\mathbf{m}} \times \frac{d\hat{\mathbf{m}}}{dt}$ term gives a spin current perpendicular to the interface (z direction) while the second term give rise to an in-plane spin current. Only the first term will be converted to the voltage across the device by ISHE effect.

In-plane rotation of the DC magnetic field is analyzed by rotation transform of the susceptibility χ from the device coordinates (x,y,z) to the lab coordinate (x',y',z') [38]

$$\Delta \mathbf{m} = R(\varphi) \chi(H) R^{-1}(\varphi) \mathbf{h} \quad (9)$$

, where $R(\varphi)$ is the rotation matrix

$$R(\varphi) = \begin{pmatrix} \cos(\varphi) & \sin(\varphi) & 0 \\ -\sin(\varphi) & \cos(\varphi) & 0 \\ 0 & 0 & 1 \end{pmatrix} \quad (10)$$

. Apply the transformation in Equation (9) (10) to Equation (6) (8) and the generalized Ohm's law gives the total measured voltage

$$V = V_{sym}L + V_{asym}D \quad (11)$$

$$\begin{aligned} V_{sym} &= \sin \Phi (V_{AMR}^x \cos \varphi \cos 2\varphi - V_{AMR}^z \cos \varphi \sin 2\varphi) \\ &\quad - V_{AHE} \cos \Phi \cos \varphi + V_{ISHE} \cos^3 \varphi \\ V_{asym} &= -\cos \Phi (V_{AMR}^x \cos \varphi \cos 2\varphi - V_{AMR}^z \cos \varphi \sin 2\varphi) \\ &\quad - V_{AHE} \sin \Phi \cos \varphi \end{aligned} \quad (12)$$

, where L and D is the symmetric and asymmetric components of the complex Lorentz function $\frac{\frac{\Delta H}{2}}{(H-H_0)+i\frac{\Delta H}{2}}$.

Device voltage measured at different metal layer thickness

The evaluation of the effective mixing conductance g_{eff} is based on the comparison of linewidth of bare V[TCNE]_x and V[TCNE]_x/Pt samples, according to the equation [3]

$$\alpha_{eff} = \alpha_0 + \frac{g\mu_B}{4\pi M_s d} g_{eff} \quad (13)$$

. We also checked the spin current conversion efficiency by comparing the ISHE voltage with various thickness of Pt layers, as shown in Figure S5 (c).

Based on one-dimensional diffusion equation

$$\frac{d^2}{dz^2} \mu_s = \frac{\mu_s}{\lambda_s^2} \quad (14)$$

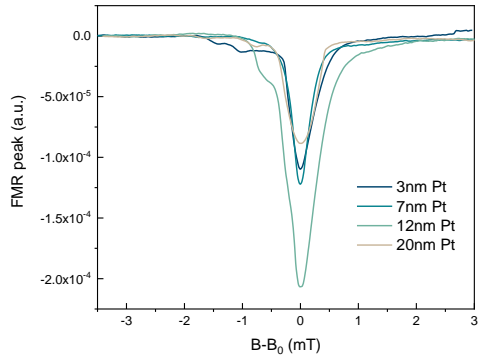
with boundary condition $j_s(0) = j_s^0$; $j_s(t_{NM}) = 0$, one may expect the measured V_{ISHE} have the thickness dependence as

$$V_{ISHE} = \frac{L\theta_{SH}\lambda_s}{\sigma_N t_{NM}} \tanh\left(\frac{t_{NM}}{2\lambda_s}\right) j_s^0 \quad (15)$$

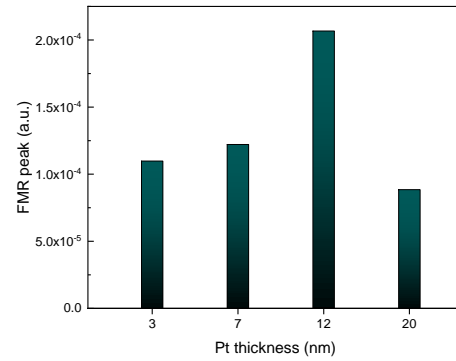
. According to previous reports $\lambda_s = 1.5nm$ in Pt layers, we indeed see the decrease in ISHE components. The decreasing rate of ISHE component is also much faster than the AMR components, which is expected to have $\frac{1}{t_{Pt}}$ dependency. However, based on the recorded

FMR signals (shown in Figure S5(a) and (b)), the quality of the film and the condition of the interface shows unneglectable batch-to-batch variation, therefore the evaluation of the λ_s and θ_{SH} based equation (15) is not practical for this device.

(a)



(b)



(c)

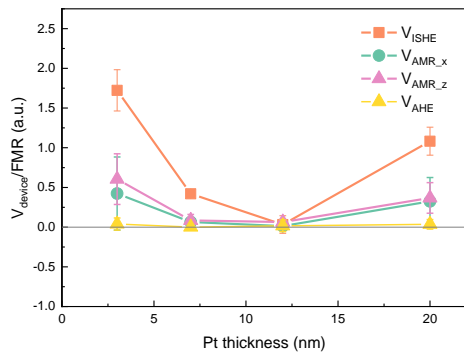


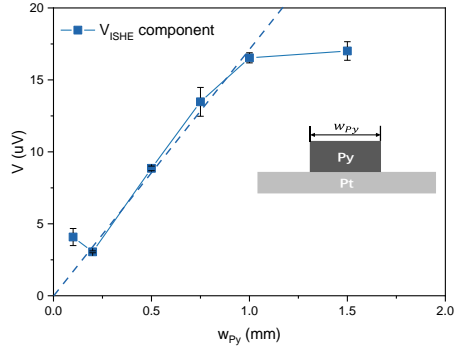
Figure S5 The Pt thickness measurement of V[TCNE]/Pt structures (a) FMR spectra (b) relative FMR peaks, and (c) V-ISHE and spin rectification effects (normalized by FMR peaks amplitudes) on bilayer samples with various Pt thickness

Width dependence data on Py/Pt, to verify the design of our coplanar waveguide

The in-plane rotation experiments require an on-chip coplanar waveguide rotating together with the sample to provide AC magnetic field. Ideal coupling the RF magnetic field to the V[TCNE]_x layer requires a uniformly distributed horizontal magnetic field above the coplanar waveguide. Non-uniform AC magnetic field may introduce incoherent magnon mode which finally dissipates as heat. To verify the design of the waveguide, we conduct a series of width dependence spin-pumping measurements on Permalloy (Py)/Pt layers, as shown in Figure S6 (a), ISHE components of the devices with Py thickness below 1 mm show good linearity with the scaling of d_{FM} . This indicates the spin current is generated uniformly within the area covered by FM layer. When $d_{FM} > 1mm$, the ISHE contribution maintain at a constant level of 20uV. This indicates the region for uniform AC magnetic field is approximately 1mm wide. In our design, the FM layer have a length of 1mm, still in the region of uniformly distributed AC magnetic field. In Figure S6, only x component of AMR increased Py width

follow same trend as ISHE, showing the larger absorbed power from the waveguide caused increase in ferromagnetic resonance, and hence increase in magnetoresistance effect, which is also of the expect.

(a)



(b)

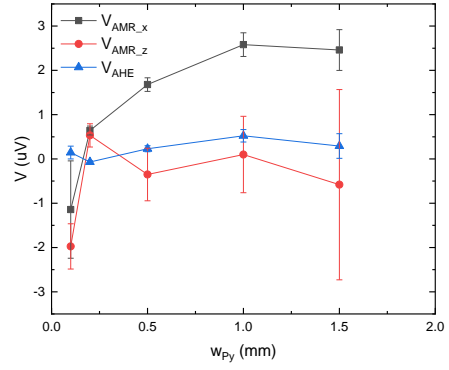


Figure S6 **Amplitudes of all components with various d_{FM} .** (a) ISHE contribution for detected spin current, (b) x,z component for anisotropic magnetoresistance effect (AMR), and anomalous Hall effect (AHE)